

Synthesis, Structural Elucidation, and Therapeutic Screening of Organotin(IV) derivatives of oxo-ethyl carbonodithioate

¹Fatima Javed, ²Saqib Ali*, ^{3,4}Khurram Shahzad Munawar, ²Ali Haider, ⁵N. A. Shah and ²Z. Rashid

¹Department of Chemistry, Shaheed Benazir Bhutto Women University, Peshawar 25000, Khyber Pakhtunkhwa, Pakistan.

²Department of Chemistry, Quaid-i-Azam University, Islamabad-45320, Pakistan.

³Institute of Chemistry, University of Sargodha, 40100, Punjab, Pakistan.

⁴Department of Chemistry, University of Mianwali, 42200, Punjab, Pakistan.

⁵Department of Biosciences, COMSATS University, Islamabad, Pakistan.

saqibali@qau.edu.pk*

(Received on 22nd March 2023, accepted in revised form 3rd August 2023)

Summary: Exploring the therapeutic potential of organotin-based oxo-ethyl carbonodithioates, a series of organotin(IV) thiocarboamates (**1-5**) were synthesized with diverse alkyl and phenyl substituents. The chemical- composition, morphology, theoretical properties, and drug-DNA binding capabilities of the synthesized derivatives were performed by applying different characterization techniques like FT-IR, NMR (¹H, ¹³C), AFM, DFT analysis, and UV-Vis spectroscopy respectively. The NMR data indicated six and four coordinated geometries, while the AFM results revealed smart surfaces concerning the grain size and root mean square (RMS) roughness, signifying catalytic and biocidal uses. The drug-DNA binding *via* intercalative mode of interaction with blue and red shifts was determined by using UV spectroscopy. The *in vitro* biocidal capacity of selected complexes was evaluated against typical bacterial, fungal, cytotoxic, and leishmanial strains respectively. As a result of the surface and biocidal characterization, the synthesized complexes may be applied with greater potential in biomedical, pharmaceutical, infectious, catalysis, and cosmetics industries.

Keywords: Organotin thiocarbonates, Surface morphology, Biocidal applications, Cytotoxicity, DFT studies.

Introduction

Structural diversity and effective biocidal activities are the characteristic features of organotin(IV) thiocarboxylates [1,2]. Several studies have successfully demonstrated the *in vivo* and *in vitro* potential of organotin complexes with potent antitumor and anticancer activities [3-6]. The surface characterization and structure activity correlation of organotin(IV) derivatives of oxo-ethyl carbonodithioate (regarding biocidal and antitumor action) must be addressed to evaluate the hi-tech biomedical and catalytic applications [7,8]. As compared to other metals, it is worth emphasizing the potential use of organotin derivatives in farming, biology, catalysis, and organic synthesis [9,10]. The capacity of organotin(IV) derivatives to bind DNA is calculated by the coordination behaviour and kind of alkyl and phenyl groups attached to the central metal ion. The success of the synthesized complexes is based on the stability of tin-based hexagonal and tetrahedral species, where nitrogen of DNA base and phosphate of DNA sugar form effective linkages with the central tin, resulting in stronger DNA bindings [11-13]. Further, The use of organometallic compounds as a medicine is very common now a days because it offers

potential advantages over the more common organic-based drugs. In addition to the advantages of high activity, compared to the platinum compound, tin complexes are much cheaper. Thus by using organotin carboxylate for clinical medicine, cost reduction, dosage reduction and effect enhancement will be reached. As per reported literature, the anticancer activity of organotin in comparison to cisplatin is much effective because of its distinct stereochemistry, dominant interaction with phosphate group of DNA, and coordinated ligand effect as investigated *in vitro* in various cancer cell line studies. The therapeutic potential of organotin complexes are also revealed. Also the Organotin(IV) compounds are characterized by high antioxidant potential by decreasing the damaging effects of oxidants through their capacity to donate one electron to the oxidant, which inhibit their oxidative activity [7,8].

Thus, the present study reports on the structural, surface, and biochemical characterization of a newly synthesized oxo-ethyl carbonodithioate ligand with antitumor, antileishmanial, and cytotoxic effects for specific applications. The study is based on the fact that organotin(IV) complexes have been characterized by

*To whom all correspondence should be addressed.

significant biocidal effects, but surface characterization and *in vitro* investigations are necessary to check the outcome of geometry and alkyl/phenyl moieties on the overall performance of compounds for hi-tech biological applications. The importance of organotin(IV) complexes to replace existing anticancer drugs like cisplatin has been determined with superior effects, so a comprehensive study is necessary to reflect the synthesis, surface characterization, and a detailed *in vitro* analysis of *oxo*-ethyl carbonodithioate derivatives as striking materials for anticancer and pharmaceutical applications [14]. Another aspect of the proposed study is to explore the effect of the toxicity of organic groups on microorganisms. The earlier reports addressed the effect in the order $R_3SnX > R_2SnX_2 > RSnX_3$ [15]. Because toxicity in the organotin compounds is thought to correspond with the total molecule surface. It is found that the *n*-butyl- and phenyl-substituted tin would be poisonous to a greater extent relative to the methyl- and ethyl-substituted tin moieties [2].

Experimental

Materials and methods

Organotin(IV) salts (Sigma, $\geq 98\%$), ethanol (Sigma, $\geq 99\%$, $M_w \approx 46.07$ g/mol), potassium hydroxide (Sigma, $\geq 99\%$, $M_w \approx 56.11$ g/mol), carbon disulfide (Sigma, $\geq 98.5\%$, $M_w \approx 76.14$ g/mol), sodium-salt of DNA (Acros $\geq 99\%$), hydrogen sulphide (Sigma, $\geq 99\%$,

$M_w \approx 34.08$ g/mol), and nitrogen gas (Acros $\geq 99.99\%$) were used as received [16]. A Bio-Cote Model SMP10 was used to record the melting points with a standard deviation of less than 0.5% over four repetitions.

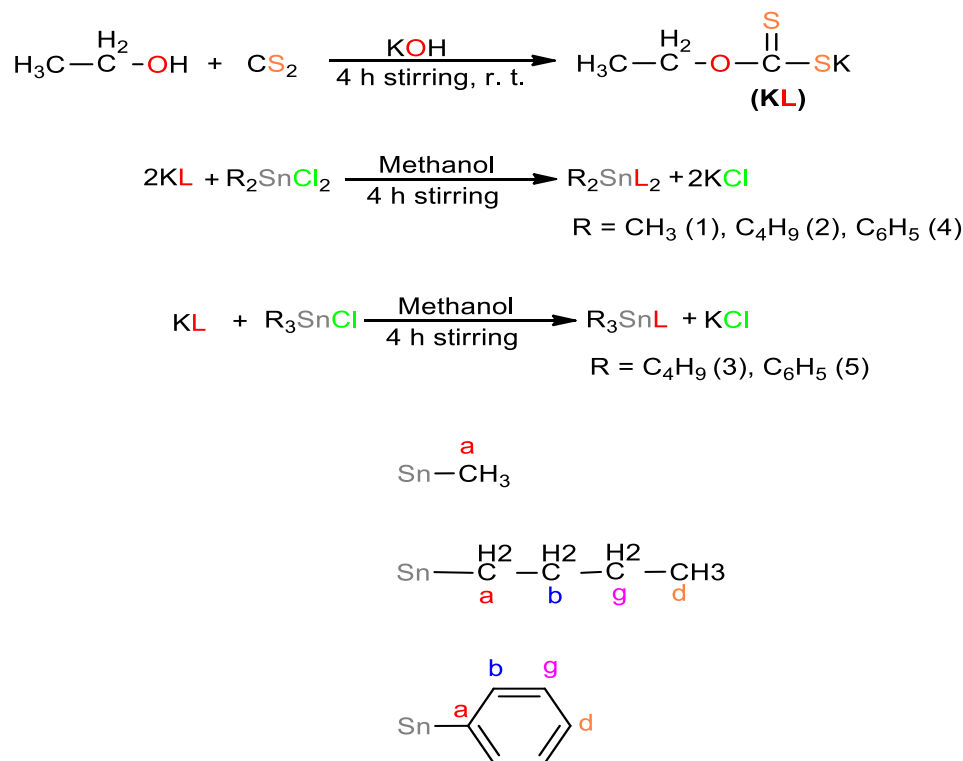
Synthesis

Synthesis of the ligand (KL)

The effective synthesis of *oxo*-ethyl carbonodithioate derivatives was performed by mixing 1 mmol of EtOH, KOH, and CS_2 with steady stirring at 25 °C for 4 hours (Scheme-1). Precipitates thus acquired were filtered, washed with EtOH, and finally dried in a desiccator for further analysis [3].

Synthesis of organotin(IV) derivatives (1-5)

Initially, 2 mmol of the potassium salt of thiocarboxylates was dissolved in 20 ml of hot MeOH, in a 50 ml double neck flask with constant stirring for 4 hours, followed by the addition of R_2SnCl_2/R_3SnCl . The products were obtained by solvent evaporation under reduced pressure at room temperature, and then organotin(IV) complexes were recrystallized from a 1:1 acetone: ether mixture. The synthetic procedure and complete numbering of the **KL** and phenyl/alkyl groups bonded to metal ion for NMR evaluation are shown in **Scheme 1**.



Scheme-1: Synthesis of organotin(IV) derivatives as well as numbering.

Characterization

FT-IR, NMR and UV-Vis analysis

A Thermo Scientific Nicolet-6700 FT-IR spectrometer was employed to acquire FT-IR data from 4000 to 250 cm^{-1} . ^{13}C and ^1H NMR spectral details of the prepared compounds were analyzed on a Bruker Avance 300 MHz NMR spectrometer with a spinning rate of 8 kHz. The correct contact duration was carefully determined according to previously documented processes to get the greatest signal-to-noise ratio and to reduce artefacts [17,18]. The UV-Vis spectrophotometer (Shimadzu 1800) was utilized to measure the absorption spectra.

Deposition of thin films

For the chemical vapor deposition method, initially, the glass substrate was properly cleaned with a mixture of acetone and petroleum (60:40 v/v), followed by vacuum drying before use. Accordingly, the temperature of the assembly was raised to 500 °C by using a controlled thermo-coupled assembly. Furthermore, the precursor was mixed with diluted H_2S flow before mixing with the chamber of the coater, and the deposition experiment was timed for 3-5 min. Finally, the glass substrate was cooled to 50 °C before being removed. The glass substrates were broken into $1.25 \times 1.25 \text{ cm}^2$ for AFM analysis. Argon gas is allowed to flow into the solution of 0.30 g of the organotin(IV) complex in 20 ml of toluene. The flask containing the solution was attached to the reactor *via* reinforced tubing. The reactor tube was positioned in a carbolite furnace with three glass substrates ($\sim 1 \text{ cm} \times 3 \text{ cm}$ and 1 mm thick) made of borosilicate, and the temperature was maintained at 400-500 °C. The precursor solution was held over a water bath on a piezoelectric modulator of a PIFCO ultrasonic humidifier in a round-bottom flask. The carrier gas carried the precursor aerosol droplets into the reactor tube. Precursor (Sn-S) fumes entered the hot substrate surface, wherein thermally persuaded reactions resulted in the deposition of the film [19]. The Sn-S description's main concern is that in the absence of H_2S flow, no coating was observed for either precursor. But after supplying a minimal flow (<1%) of H_2S , all the precursors produced Sn-S films at substrate temperatures of around 500 °C. The growth rates of selective films were observed in the 200-300 nm range per min, which is comparable to the corresponding reaction of SnCl_4 with H_2S [20].

Elemental analysis and Atomic Force Microscopy

A LECO CHNS-932 analyzer was used to determine the quantitative levels of C, H, and S. Under tapping mode, the phase and topography of Sn-S-based thin films were explored utilizing a V-shaped Si_3N_4 cantilever (HYDRA6V, USA) with a tip radius of 30 nm and a spring constant of 0.3 N/m for imaging soft samples. The samples were adhered to a typical microscopic slide utilizing blue-light triggered glue and put on the sample stage of a Benyuan CSPM 5500 Scanning Probe Microscope. During laser synchronization, the imaging sensing performance was calibrated, and the grain size, surface, and RMS were determined by employing the MFP-3D software [21].

Theoretical study

Gaussian09 package was used for density functional theory (DFT) calculations. A 6-31G* basis set for S, O, C, and H was used in all computations. This basis set adds d-type polarisation functions to the first and second-row elements. For the Sn atom, LANL2DZ basis set was used, which employs the Los Alamos effective core potential on the metal atom. The geometries of the compounds (1–5) were optimized using DFT/B3LYP method. No compound was subjected to any symmetry constraint throughout the geometry optimization process. The subsequent Hessian calculations proved that the optimized structures represent local minima on the potential energy surface as no imaginary frequencies were discovered in any scenario.. GaussView was used to visualize the HOMO-LUMO isosurface plots and the geometries of the optimized structures.

Drug DNA interaction and Biological screening

Accordingly, a stock solution of DNA in 10 mmol/dm^3 phosphate buffer (pH = 7.0) was prepared, and the concentration was estimated by measuring absorbance at 260 nm after 1:100 dilutions. The molar absorption coefficient was set at $6600 \text{ mol}^{-1}\text{cm}^{-1}$, and the solution was placed at a temperature below 4 °C at the stationary level before being analyzed with the help of a UV-Vis spectrophotometer. By adding tiny aliquots of the DNA solution, the spectroscopic feedback of the same quantity of the organotin complex was then observed. UV-Vis spectroscopy was employed to find out the drug-DNA binding constants (K) using Equation I [23].

$$\frac{A_0}{A - A_0} = \frac{\epsilon_G}{\epsilon_{H-G} - \epsilon_G} + \frac{\epsilon_G}{\epsilon_{H-G} - \epsilon_G} \frac{1}{K[\text{DNA}]} \quad (\text{I})$$

The value of K is given by the intercept-to-slope ratio of the plot $1/[DNA]$ vs $A_0/A - A_0$.

Biological screening

The screening experiments were carried out using the same protocols as previously described [3].

Results and discussion

Physical characteristics of organotin(IV) complexes

All of the organotin derivatives solids have sharp melting points and considerable solubility in typical solvents. Table 1 contains physical details and elemental analysis data.

FT-IR spectra

The chemical structures of synthesized derivatives (**1-5**) have been confirmed by FT-IR analysis, which is given in **Table 2**. The shifting of the absorption band from 1355 to 1206–1290 cm^{-1} was detected in the overall spectra of the organotin(IV) derivatives, which verified the effective coordination *via* the thiolate sulfur with the tin atom. The absorption bands for $\nu(\text{Sn-S})$ from 358 to 375 cm^{-1} also suggested real coordination of the dithio ligand with the Sn atom. Further, the interactions in terms of monodentate and bidentate complexation between the respective ligand and Sn atom could be verified by FT-IR stretching frequencies. In the overall spectra, the asymmetric $\nu(\text{CSS})_{\text{as}}$, and symmetric $\nu(\text{CSS})_{\text{s}}$ absorption frequencies were detected between 1206–1355 cm^{-1} and 1008–1079 cm^{-1} , correspondingly. The

realization of FT-IR analysis proved the bidentate mode of interaction for the complexes (**1**), (**2**), and (**4**), along with the monodentate mode for complexes (**3**) and (**5**), at $\Delta\nu \approx 198, 181, 266, 160,$ and 252 cm^{-1} , respectively. The increase in $\Delta\nu$ for complexes (**3**) and (**5**) is attributed to the steric hindrance effect of tributyl and triphenyl groups [24], as supported by theoretical studies. The (Sn-C) peak was observed in complexes (**1**), (**2**), and (**3**) between 548 to 592 cm^{-1} , but in the derivatives (**4**) and (**5**), the same band was detected at 279 and 260 cm^{-1} because of the planar and conjugate behaviour of the phenyl ring. These results are reliable with those obtained for several comparable organotin(IV)-sulfur donor ligands [25]. The FT-IR spectra also showed the characteristic sharp band for (C-O-C) in the section from 971 to 999 cm^{-1} . Based on analysis of the infrared details of the **KL** and its coordinated complexes, it is proposed that it binds with the Sn ion in either mono or bidentate fashion depending on the types of groups attached.

NMR spectral studies

Table-3 shows the NMR data of the synthesized derivatives (1-5). ^1H NMR data was executed to inspect the respective peaks in terms of multiplicity, integration, and appearance of satellite peaks to assess the structural features of synthesized compounds. The absence of a SH peak due to deprotonation of the ligand confirms the complex formation [26]. The downfield shift in the position of $-\text{C}_2\text{H}_5$ protons was observed on the attachment of the sulphur atom with the metal atom, as reported in the literature [27,28].

Table-1: Physical details of KL and its corresponding organotin(IV) derivatives.

Compounds	Molecular Formula	Molecular mass	Yield(%)	Melting Point ($^{\circ}\text{C}$)	Elemental Analysis % Calculated (Found)		
					C	H	S
KL	$\text{C}_3\text{H}_5\text{KOS}_2$	159.94	80	207-208	22.48 (22.39)	3.14 (2.99)	40.04 (39.05)
(1)	$\text{C}_8\text{H}_{16}\text{O}_2\text{S}_4\text{Sn}$	391.91	72	102-103	24.56 (24.44)	4.12 (3.85)	32.79 (32.01)
(2)	$\text{C}_{14}\text{H}_{28}\text{O}_2\text{S}_4\text{Sn}$	476.00	78	109-111	35.37 (35.35)	5.94 (5.55)	26.98 (26.59)
(3)	$\text{C}_{15}\text{H}_{32}\text{OS}_2\text{Sn}$	412.09	70	111-113	43.81 (43.30)	7.84 (7.57)	15.59 (15.10)
(4)	$\text{C}_{18}\text{H}_{20}\text{OS}_4\text{Sn}$	499.94	75	122-124	43.30 (42.79)	4.04 (4.01)	25.69 (25.48)
(5)	$\text{C}_{21}\text{H}_{20}\text{OS}_2\text{Sn}$	484.23	70	93-94	43.81 (43.50)	7.84 (7.20)	15.59 (14.20)

Table-2: FT-IR spectral details of the synthesized compounds.

Compounds	FT-IR Peaks (cm^{-1})					
	$\nu(\text{CSS})_{\text{asym}}$	$\nu(\text{CSS})_{\text{sym}}$	$\Delta\nu$	$\nu\text{C-O}$	$\nu\text{Sn-S}$	$\nu\text{Sn-C}$
KL	1355	1070	285	999	-	-
(1)	1206	1008	198	979	358	548
(2)	1259	1078	181	971	360	578
(3)	1290	1024	266	981	366	594
(4)	1214	1054	160	996	370	280
(5)	1260	1008	252	966	375	261

Table-3: ^1H NMR spectroscopic data ^{a-c}.

Compounds	H1	H2	α	β	γ	δ
KL	1.17 (7.2)	4.63 (q, 7.2)	-	-	-	-
(1)	1.43 (m)	4.52 (q, 7.2)	1.47 [s, 79, 75]	-	-	-
(2)	1.43 (m)	4.51 (q, 7.2)	2.02 (m)	1.87 (m)	1.39 (m)	0.92 (t, 7.2)
(3)	1.39 (m)	4.49 (q, 7.2)	1.59 (m)	1.34 (m)	1.30 (m)	0.89 (t, 7.2)
(4)	1.25 (7.2)	4.35 (q, 7.2)	-	7.99 (m)	7.54 (m)	7.49 (m)
(5)	1.08 (7.2)	4.35 (q, 7.2)	-	7.76 (m)	7.50 (m)	7.46 (m)

^aSee Scheme 1 – for numberings and α , β , γ , δ .

^bChemical shifts (δ) in ppm. $^3J(^1\text{H}, ^1\text{H})$ and $^nJ(^{117/119}\text{Sn}, ^1\text{H})$ in Hz are itemized in parenthesis and square brackets, respectively.

^cMultiplicity is represented as, s = singlet, m = multiplet, q = quartet, t = triplet,

Table-4: ^{13}C NMR details of the synthesized compounds ^a.

Compounds	Carbon No.						
	C1	C2	C3	α	β	γ	δ
KL	14.9	66.5	230.3	-	-	-	-
(1)	13.9	72.2	221.7	10.42 [594, 569]	-	-	-
(2)	13.9	72.1	222.8	30.4 [538, 514]	28.8 [40]	26.4 [117, 114]	13.7
(3)	13.6	70.9	217.5	15.6 [335, 320]	28.6 [22]	27.0 [66, 62]	13.9
(4)	13.3	71.7	214.4	141.5 [850, 806]	129.1 [85]	135.3 [58]	130.2 [18]
(5)	13.6	72.5	218.5	138.0 [588, 560]	129.1 [61, 60]	136.6 [46]	130.0 [13]

^aChemical shifts (δ) in ppm. $^nJ(^{119/117}\text{Sn}, ^{13}\text{C})$ in Hz is given in the square bracket

Table-5: Sn-C coupling (Hz) details of the synthesized compounds.

Complex. No.	$^1J(^{119}\text{Sn}, ^{13}\text{C})$ (Hz)	$^2J(^{119}\text{Sn}, ^1\text{H})$ (Hz)	Angles ($^\circ$)	
			1J	2J
(1)	594	79	129	125
(2)	539	-	129	-
(3)	335	-	108	-
(4)	850	-	112	-
(5)	588	-	129	-

Using the coupling constant [$^2J(^{119/117}\text{Sn}, ^1\text{H})$], compound (1) was observed with a hexagonally coordinated Sn atom at 75 and 79 Hz, whereas compounds (2) and (3) were observed with a clear triplet at 0.92 and 0.89 ppm due to terminal methyl groups. Further, in complex (3), a strong shielding effect was observed due to the existence of n-butyl with Sn atoms through carbon nuclei [29]. The calculated geometry of triphenyltin(IV) was similar to the monodentate bonding of the 1,1-dithiolate group in the solution [27]. According to the reported literature [30], the phenyl peaks in complexes (4) and (5) were observed as two discrete sets, with one region assigned to the thiocarboxylate ligand ($\delta = 1.08$ – 4.35 ppm) and the other to the triphenyltin moiety ($\delta = 7.46$ – 7.99 ppm). The ^1H NMR analysis suggested ortho protons with downfield at $\delta = 7.69$ and 8.00 ppm and the respective meta and para protons with upfield at $\delta = 7.42$ – 7.50 ppm.

^{13}C NMR analysis of the synthesized ligand and its derivatives (1-5) is specified in Table 4. A significant chemical shift of carbon in the dithiocarbonate compound is thion carbon (CS_2). The peak observed for CS_2 at $\delta = 230.3$ ppm in the ligand was shifted to $\delta = 221.7$, 222.8 , 217.5 , 214.4 , and 218.5 ppm in the corresponding tin complexes (1-5), which verified the effective linking of the ligand with the central metal [31]. The upfield shift is suggested by an increase in

electron density because of the mobilization of the lone pair of oxygen in OCS_2 . From the analysis, it was concluded that tin resonance is intensely reliant on features including concentration, temperature, and electronegativity of the ligand under investigation. The results revealed an escalation in the coordination number of the Sn after complexation in comparison to the ligand. The coupling constant $^1J(^{119}\text{Sn}, ^{13}\text{C})$ and the corresponding θ (C-Sn-C angle) values determined from Lockhart's equation ($^1J = 10.7\theta - 778$) were employed to find out the coordination number of Sn [32]. Table 5 shows the calculated values for complexes (1) 594 Hz (129°), (2) 538 Hz (129°), and (4) 850 Hz (112°) to confirm the six coordinated Sn, while complex (3) 335 Hz (108°) suggested the four-coordinated Sn [3]. The peak observed at 138 ppm is attributed to ipso-carbon verifying the four-coordinated geometry of Sn in triphenyl derivatives [28].

Atomic force microscopic analysis (AFM)

The surface morphology and structural analysis of organotin derivatives were analyzed in tapping mode by means of atomic force microscopy. AFM can be utilized to define two- and three-dimensional topographic features, as well as to measure pore size and RMS roughness of organotin complexes [33]. Thin films of organotin derivatives (Sn-S) were obtained on the

surface of glass substrates with the help of toluene solution by the chemical vapour deposition technique (CVD). Representative complexes (1-3 and 5) were selected as the precursors for CVD trials [34]. Substrate temperatures < 400 °C were insufficient to commence Sn-S deposition, so the film deposition temperature was adjusted between 400 and 555 °C [33]. The brownish-yellow adherent film was formed in the range of 430-450 °C for the representative complexes, while dark black films were produced at 470 and 500 °C. In CVD analysis, the creation of Sn-S films defined the simple reduction of metal centre Sn(IV) to Sn(II) in an argon environment. AFM images of the representative complexes are shown in Fig 1. AFM scans revealed significant microstructural features about its grain size. The grains that have been detected are triangular and symmetric. Two kinds of grains were seen, with one type having a measured width of 370 nm and a length of 875 nm and the other having a width of 560 nm and a length of 980 nm. A much larger grain size suggested the capability of Sn-S thin films, which could be used for a variety of adsorption and bioseparation processes. To investigate the surface overview, the RMS roughness was observed in the range of 300-750 nm. The determined roughness indicated the competence of Sn-S thin films as a potential candidate for a variety of reaction engineering and heterogeneous catalysis [35].

DFT Studies

The DFT-calculated geometric parameters of synthesized complexes are given in Table 6. The optimized structures, Highest Occupied Molecular Orbital (HOMO) and Lowest Unoccupied Molecular Orbital (LUMO) plots of the organotin derivatives are given in Figs 2 and 3.

According to the computational analysis, complexes (1), (2), and (4) have a bidentate mode of coordination *via* thiolic sulphur adapting distorted octahedral geometry, whereas complexes (3) and (5) have a unidentate mode of coordination *via* tetrahedral geometry. The statement was also confirmed by the demonstration of bond angles in distorted octahedral and tetrahedral geometries. Table 6 presents the investigated bond distances

(2.617, 2.628, 2.505, 2.606, and 2.487 (Å)) of Sn-S in complexes (1-5) that are in close agreement with the earlier reports [36]. The bond angles in derivative (1) are [C(2)-Sn(1)-C(4) = 109.17°, [C(4)-Sn(1)-S(5) = 101.90°, [S(3)-Sn(1)-S(5) = 148.09°], in derivative (2) [C(2)-Sn(1)-C(4) = 111.56°, [C(4)-Sn(1)-S(5) = 99.0°], [S(3)-Sn(1)-S(5) = 147.92°], in derivative (3) [C(2)-Sn(1)-C(5) = 115.75°, [Sn(1)-S(5)-C(7) = 88.97°], [Sn(1)-S(5)-C(11) = 122.48°], in derivative (4) [C(2)-Sn(1)-C(4) = 105.83°, [C(4)-Sn(1)-S(5) = 101.84°], [S(3)-Sn(1)-S(5) = 149.08°], and [C(2)-Sn(1)-C(5) = 114.09°], [S(3)-Sn(1)-C(5) = 116.04°], [S(3)-Sn(1)-C(4) = 95.83°] in derivative (5) that are close to those stated for tin complexes derived from thiohydrazones [37]. To investigate the structure-property relations of such complexes, HOMO and LUMO energies were calculated [38]. The results suggest that HOMO is directly linked with the ionization potential, whereas LUMO is directly proportional to the electron affinity. The "energy gap" is the difference between the HOMO and LUMO orbitals, which is a fundamental aspect of studying structural stability [39]. The high values of HOMO refer to more reactive interactions with electrophiles, whereas lower LUMO is essential for molecular reactions. The energy gap between HOMO-LUMO also suggests the hard or soft nature of molecules for specified applications. Further, the high energy gap presents hard molecules with less reactivity as compared to soft molecules with small energy gaps. This happens as soft molecules are more polarisable and need small energy for excitation [40,41]. Thus, it is clear that the LUMO orbital is focused on the Sn atom, verifying the nucleophilic attack, while the HOMO is localized over the sulphur moiety. Thus, a smaller HOMO-LUMO energy gap might clarify charge transfer inside the molecules. As summarized in Table 7, complexes (1-5) are stable, as indicated by HOMO-LUMO gap values [38]. Chemical hardness (*h*) reflects the resistance to charge transfer and is a good indicator of chemical stability; however, global softness (*S*) is related to the polarizability of synthesized complexes [42,43]. Consequently, charge transfer resistance was shown by complexes, as observed from the values of η and *S*.

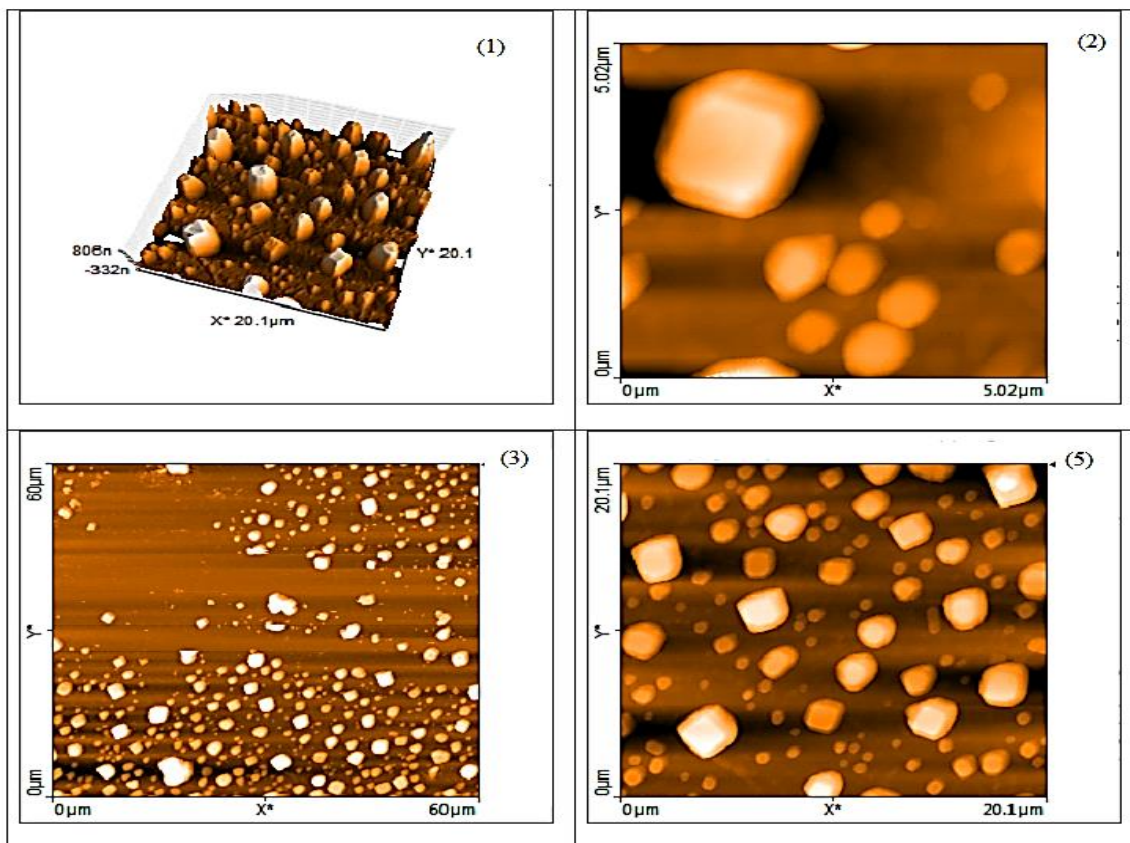


Fig. 1: Surface characterization of complexes (1-3) and (5) by AFM analysis at pH = 7.45 and T = 25 °C.

Table-6: Optimized bond distances (Å), bond angles (°), and torsion angles in the derivatives (1-5).

Complex. No.	Bond distances (Å)		Bond angles (°)		Torsion angles (°)	
(1)	Sn1-C2	2.152	C2-Sn1-C4	109.17	C2-Sn1-C4-S5	101.23
	Sn1-S3	2.617	C4-Sn1-S5	101.90	S3-C4-Sn1-S5	153.76
	Sn1-C4	2.152	S3-Sn1-S5	148.09	S3-Sn1-C2-S9	65.35
	Sn1-S5	2.617	Sn1-S3-C6	89.10	Sn1-S5-C7-O10	177.87
	Sn1-S11, S5-C7	2.852, 1.730	Sn1-S5-C7, S5-C7-S11	89.09, 122.24	S3-C6-S9-Sn1, S3-S9-C6-O8	2.36, 179.54
	(2)	Sn1-C2	2.172	C2-Sn1-C4	111.56	C2-Sn1-C4-S5
Sn1-S3		2.628	C4-Sn1-S5	99.00	S3-C4-Sn1-S5	153.33
Sn1-C4		2.173	S3-Sn1-S5	147.92	S3-Sn1-C2-S9	64.83
Sn1-S5		2.629	Sn1-S3-C6	88.90	Sn1-S5-C7-O10	177.80
Sn1-S11, S5-C7		2.858, 1.729	Sn1-S5-C7, S5-C7-S11	88.97, 122.48	S3-C6-S9-Sn1, S3-S9-C6-O8	3.15, 179.49
(3)		Sn1-C2	2.157	Sn1-S3-C6	102.25	S3-Sn1-C2-C5
	Sn1-S3	2.503	S3-C6-S8	126.53	C2-Sn1-C4-C5	129.19
	Sn1-C4	2.167	S3-C6-O7	108.56	C2-Sn1-S3-C6	-65.40
	Sn1-C5	2.157	C2-Sn1-C5	115.75	S3-C6-S8-O7	-179.95
	S3-C6, C6-S8	1.766, 1.667	S3-Sn1-C5, S3-Sn1-C4	111.41, 97.04	S8-C6-O7-C9, C6-O7-C9-C10	0.02, 179.01
	(4)	Sn1-C2	2.151	C2-Sn1-C4	105.83	C2-Sn1-C4-S5
Sn1-S3		2.606	C4-Sn1-S5	101.84	S3-C4-Sn1-S5	155.13
Sn1-C4		2.151	S3-Sn1-S5	149.08	S3-Sn1-C2-S9	66.22
Sn1-S5		2.606	Sn1-S3-C6	88.62	Sn1-S5-C7-O10	177.61
Sn1-S11, S5-C7		2.825, 1.730	Sn1-S5-C7, S5-C7-S11	88.57, 122.22	S3-C6-S9-Sn1, S3-S9-C6-O8	2.43, 179.69
(5)		Sn1-C2	2.129	Sn1-S3-C6	102.95	S3-Sn1-C2-C5
	Sn1-S3	2.487	S3-C6-S8	126.59	C2-Sn1-C4-C5	125.07
	Sn1-C4	2.143	S3-C6-O7	108.15	C2-Sn1-S3-C6	-66.36
	Sn1-C5	2.135	C2-Sn1-C5	114.09	S3-C6-S8-O7	179.41
	S3-C6, C6-S8	1.770, 1.662	S3-Sn1-C5, S3-Sn1-C4	116.04, 95.83	S8-C6-O7-C9, C6-O7-C9-C10	-0.16, -179.51

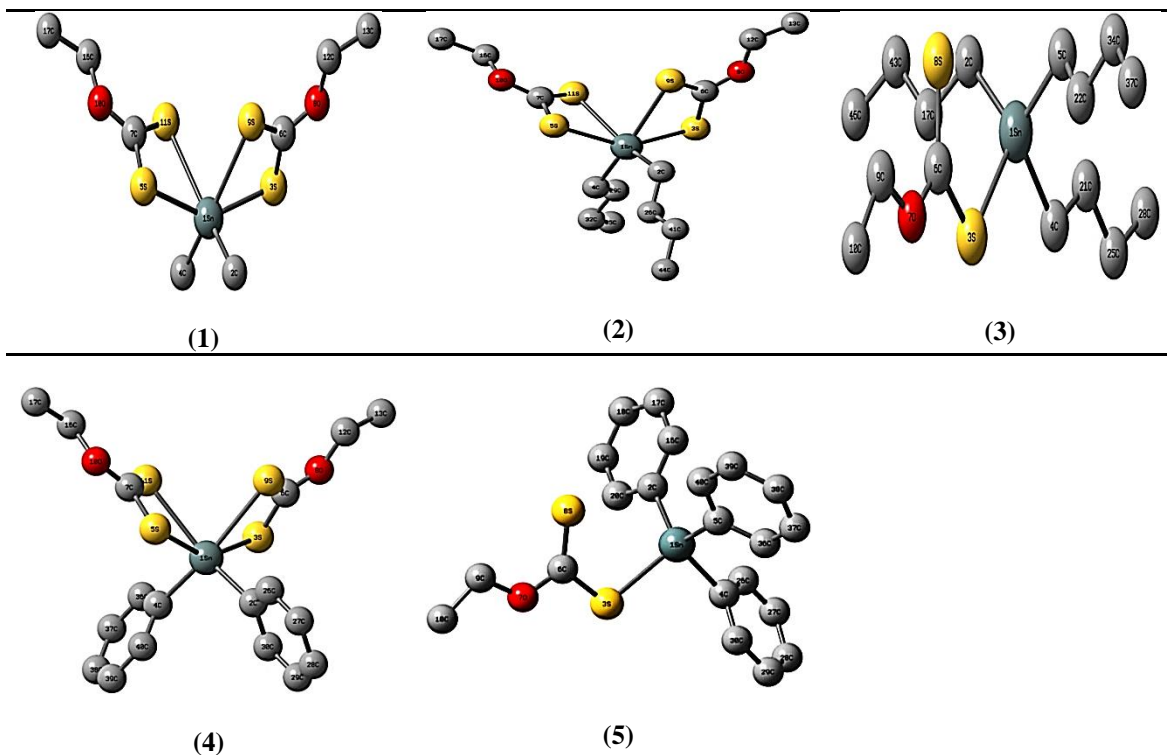
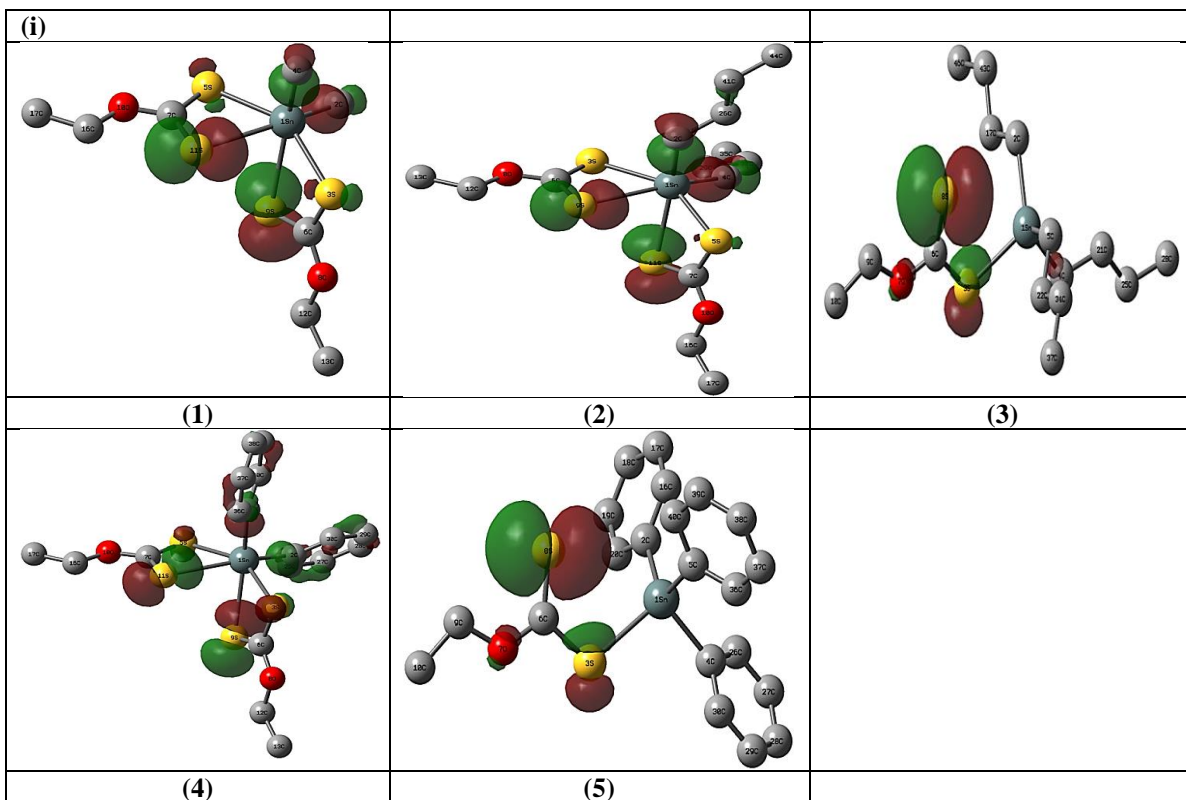


Fig. 2: DFT/B3LYP optimized structures of derivatives (1-5). Hydrogen atoms are omitted for clarity.



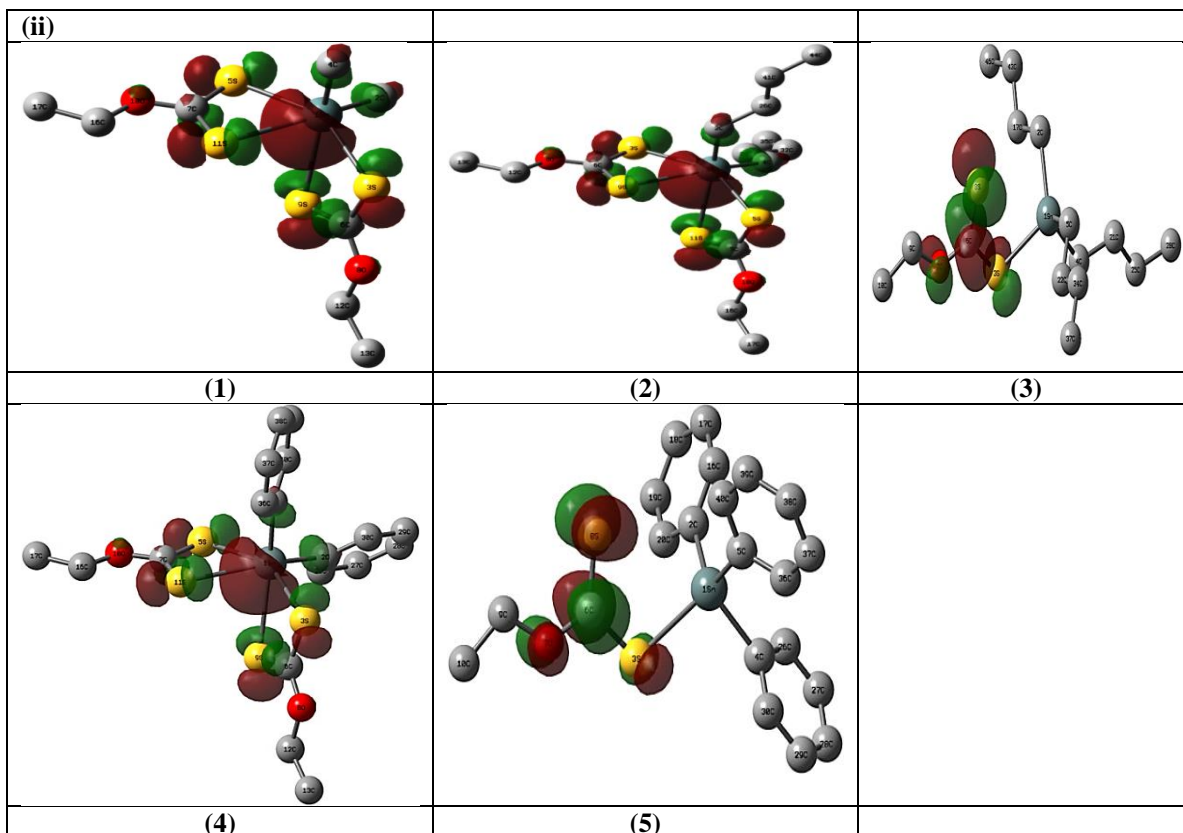


Fig. 3: The HOMO (i) and LUMO (ii) plots for derivatives (1-5).

Table-7: Energy gap (HOMO-LUMO), hardness, softness, and dipole moment values of the complexes (1-5).

Complex. No.	HOMO (eV)	LUMO (eV)	HOMO-LUMO gap(eV)	Global Hardness (η , eV)	Global Softness (S, eV ⁻¹)	Dipole Moment (debyes)
(1)	-6.35168	-1.74697	-4.60471	3.251	0.13122	2.446
(2)	-6.13508	-1.65091	-4.48416	3.264	0.1445	2.742
(3)	-6.40066	-1.75758	-4.64308	3.267	0.14876	2.654
(4)	-6.00745	-1.11893	-4.88852	3.213	0.15084	2.483
(5)	-6.03739	-1.14206	-4.89533	3.531	0.13845	1.363

Biological activities

DNA binding studies

In vitro binding interactions of metal derivatives to DNA were investigated by using UV-visible spectroscopic absorption titration followed by a variation in absorbance with a shift in the respective wavelength, as shown in Fig 4. The spectroscopic analysis suggested a single absorption band in the range of 268 to 311 nm for all derivatives because of the n- π^* transition of coordinated compounds. By increasing the concentration of DNA, hypochromism as well as the bathochromic shift is perceived. The studies revealed that phenomena of hyperchromism and hypochromism were observed, which are referred to as spectral changes due to the association of the metal complex with the DNA helix. Both shifts were consistent owing to the interaction of π electrons of the compounds with π electrons of nitrogenous bases present in the DNA strand. A redshift was observed

due to a decrease in the transition between π - π^* electrons in the overall system [44,45]. To calculate the binding ability of complexes with DNA, the intrinsic binding constant was calculated with the help of the Benesi-Hildebrand equation [6,7].

For ligand and complexes, the binding constants (4.3×10^5 , 6.4×10^5 , 1.5×10^3 , 9.9×10^5 , and 4×10^6 M⁻¹) suggested the complex (5) with a higher binding strength. As shown in Table 8, Gibb's free energy of the KL and derivatives (1-5) were obtained with the help of Equation II [4,8].

$$\Delta G = -RT \ln K \quad (\text{II})$$

where "R" is the general gas constant (8.314 JK⁻¹mol⁻¹) and T is the temperature (298 K). The Gibb's free energies are -18.6, -14.9, -15.1, -17.1, -20.0, and -20.9 kJ mol⁻¹ for the ligand and complexes (1-5), respectively, which proposes that the interactions of samples with DNA are spontaneous [9].

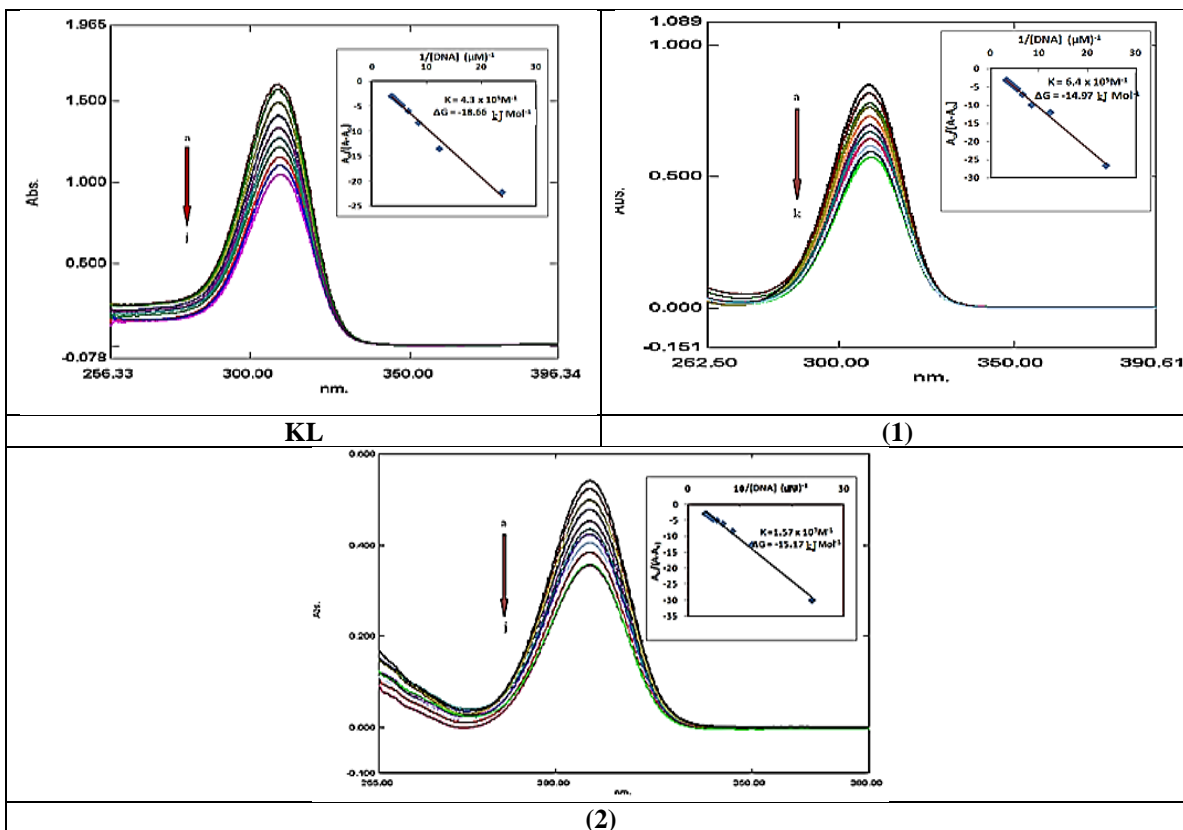


Fig. 4: UV-Vis spectroscopic response of 0.8 mmol L⁻¹ KL, (1) and (2) in the absence and presence of (a) 20 (b), 40 (c), 62 (d), 83 (e) 104 (f), 125 (g), 150 (h), 170 (i), 192 (j), and 222 (k) μM DNA.

Table-8: Binding constant and Gibbs free energy of the synthesized compounds.

Compounds	K (M ⁻¹)	-ΔG (kJ mol ⁻¹)
KL	4.3 × 10 ⁵	18.6
(1)	6.4 × 10 ⁵	14.9
(2)	1.5 × 10 ⁵	15.1
(3)	9.9 × 10 ⁵	17.1
(4)	1.7 × 10 ⁶	20.0
(5)	4.0 × 10 ⁶	20.9

Antibacterial activity

The organotin-based *oxo*-ethyl carbonodithioate derivatives were investigated for antibacterial potential by the agar well diffusion method in the presence of Cefixime as a standard drug [46]. KL showed antibacterial activity only against the *M. luteus* strain, which is a gram-positive bacteria, but no activity was noted against *Gram negative* strain bacteria, i.e., *E. coli* and *B. bronchiseptica*. However, complexes 1-5 exhibited noteworthy activity against both the *Gram positive* and *Gram negative* strains. Overall, maximum zones of inhibition were observed against *Gram positive* strains relative to *Gram negative* strains. In the case of *B. subtilis*, complex (3) showed an equal zone of inhibition to control cefixime.

The results suggested that all of the complexes indicated a momentous activity towards the tested strains. The antibacterial activity in terms of the structure activity correlation is attributed to the tetrahedral geometry of organotin-based *oxo*-ethyl carbonodithioate derivatives, an increase in alkyl functionalities, and the hydrophilic nature of the ligand. Consequently, the increase in lipophilicity due to the delocalization of electrons on tin tends to increase the permeability through the cell membrane [47]. The antibacterial activity of synthesized complexes is shown in Fig 5.

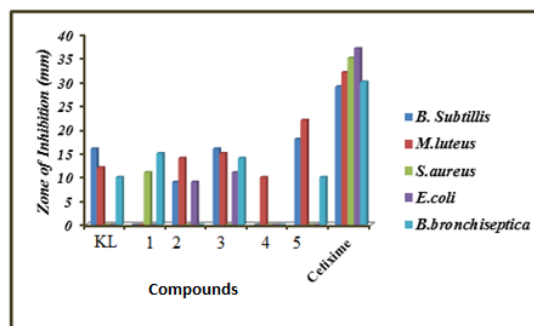


Fig. 5: Antibacterial activity of KL and its derivatives

Antifungal activity

To check the antifungal potential of synthesized derivatives (1-5), Terbinafine was selected as a standard drug against fungal strains like *Fusarium solani*, *Mucor species*, *Aspergillus niger*, *Aspergillus flavus*, and *Helminthosporium solani* by means of the agar dilution method. From the data presented in Fig 6, complexes (3) and (5) exhibited maximum activity towards all fungal strains, whereas complexes (1) and (4) disclosed non-significant activity because tri organotin compounds are more bioactive than di organotin analogues [48,49].

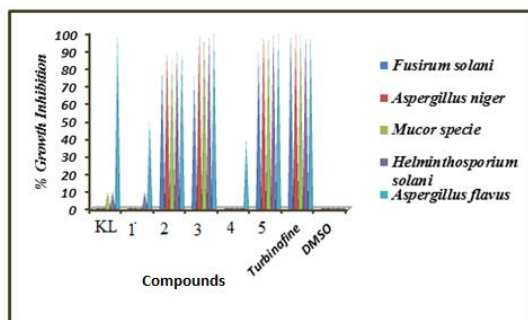


Fig. 6: Antifungal activity of KL and its derivatives.

Cytotoxic activity

The cytotoxic studies of organotin(IV) derivatives were calculated by the brine-shrimp assay, as shown in Fig 7. The detailed studies suggested the noticeable biological activity of organotin(IV) derivatives owing to the passage of more active species ($[R_nSn_{(4-n)}]^+$, where $n = 2$ or 3) across the cell membrane [50]. As per the reported literature, the cytotoxic effect is more pronounced if the

LD_{50} value is below 20-30 $\mu\text{g/ml}$ [4]. In comparison to standard drugs, all the derivatives presented low cytotoxicity. However, among synthesized compounds, complex 3 exhibited the highest cytotoxicity, followed by KL, and complex 4 showed the lowest toxicity. The outcomes disclosed that the triorganotin derivatives have higher toxicity than diorganotin, which is in close agreement with the earlier findings [51]

Antileishmanial activity

Additionally, the KL and synthesized derivatives were investigated against pathogenic Leishmania. The standard drug was Amphotericin B ($0.048 \mu\text{g ml}^{-1}$). The results suggested a higher activity of organotin(IV) complexes concerning KL and addressed the dynamic part of tin regarding antileishmanial performance. The antileishmanial activity follows the following order in efficacy: Bu_3SnL (3) $>$ Ph_3SnL (5) $>$ Bu_2SnL_2 (2) $>$ Ph_2SnL_2 (4) $>$ Me_2SnL_2 (1), as shown in Fig 8, respectively. To reflect the structure-activity relationship, this performance is attributed to the degree of coordination, lipophilicity, planarity, molecular weight, number of alkyl/phenyl fragments, and geometry around tin [52]. Accordingly, four-coordinated organotin derivatives were more active than six-coordinate ones. Complexes (3) and (5) were observed with higher activity with reasonable cytotoxicity LD_{50} values of 0.0023 and 0.0025 $\mu\text{g ml}^{-1}$, correspondingly. The marked activity was due to the presence of planner phenyl rings, which can enter effortlessly into the cell membrane. The results addressed such complexes as a new class of antileishmanial drugs.

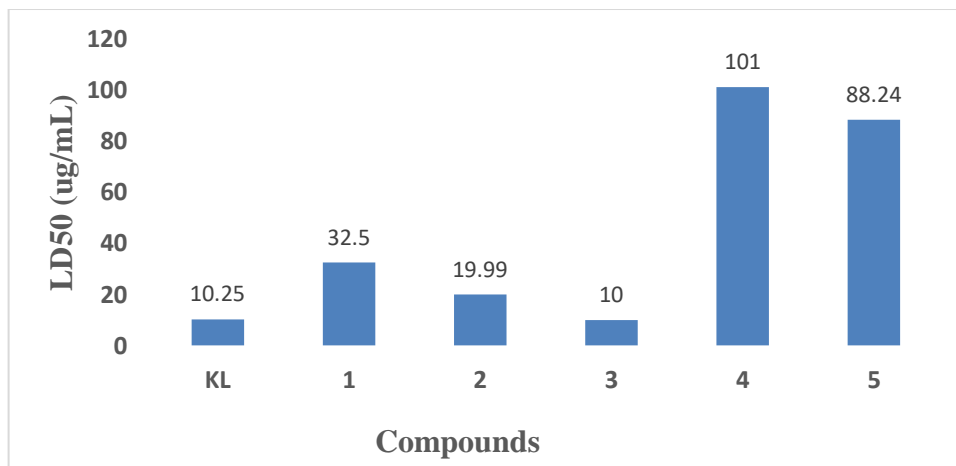


Fig 7: *In vitro* cytotoxic activity of KL and its corresponding derivatives against brine shrimps.

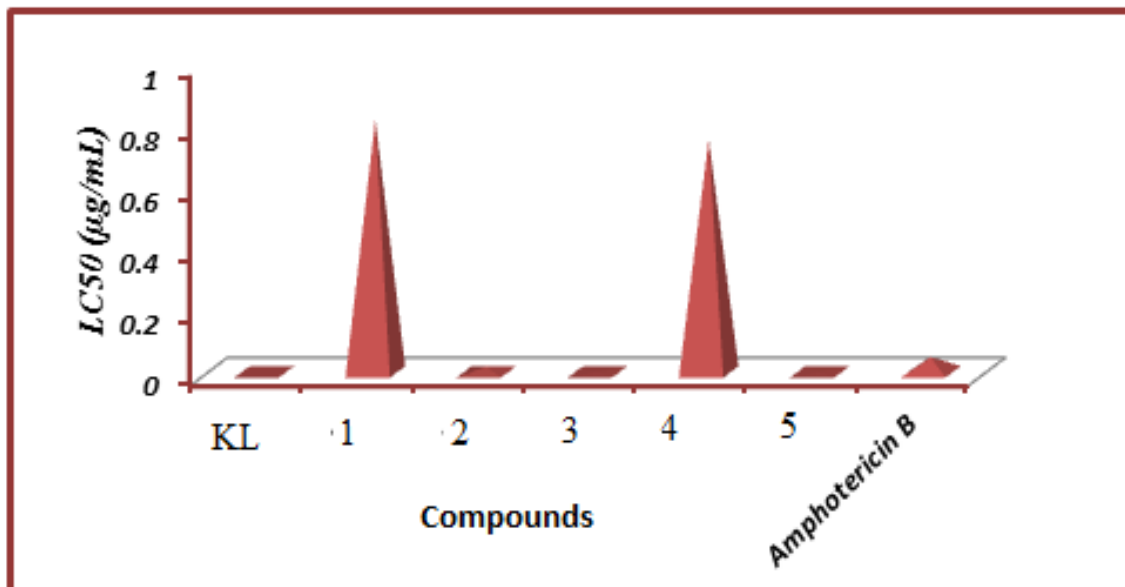


Fig. 8: Antileishmanial activity of **KL** and its corresponding complexes.

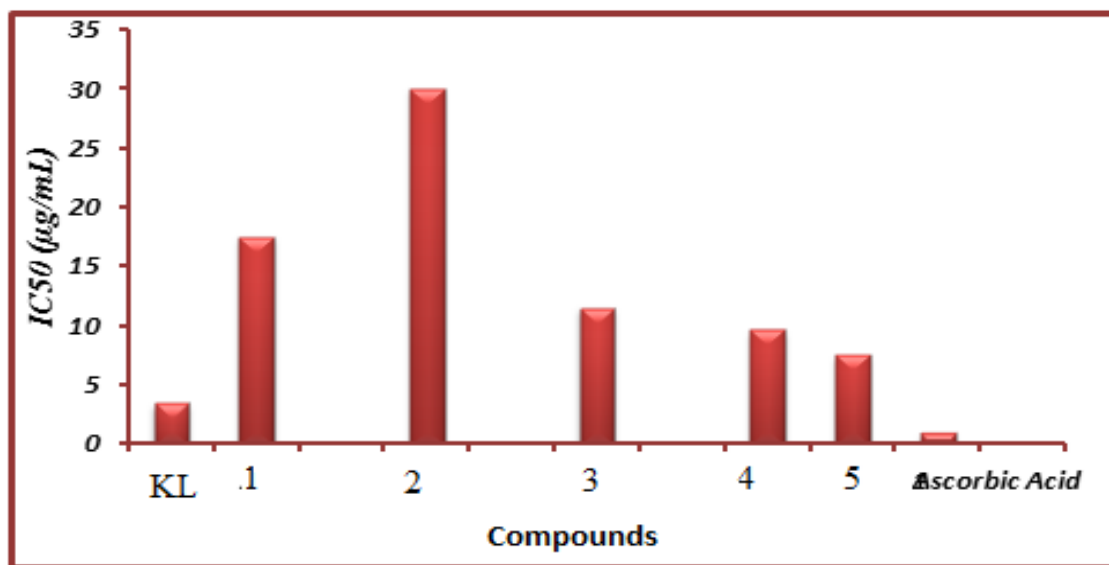


Fig. 9: Antioxidant scavenging assay of **KL** and its corresponding complexes.

Antioxidant activity

By observing how different quantities of the free stable radical 1,1-diphenyl-2-picrylhydrazyl (DPPH) interacted with the complexes of organotin(IV), the antioxidant properties of these compounds were also investigated, as reported earlier [53]. According to the findings, raising the concentration of the tested samples causes the radical's absorption intensity to rapidly decrease. The effects of the **KL** and its derivatives were investigated in contrast

to the standard antioxidant ascorbic acid. When compared to the standard drug, the examined complexes were shown to have reasonable antioxidant activity. As shown in Fig 9, the highest activity was observed for free ligand **KL** in comparison to complexes but was lower than standard ascorbic acid.

Protein kinase inhibition activity

A preliminary analysis of protein kinase activity was performed for the synthesized complexes,

which is considered a preliminary assay of antitumor activity. Regarding kinase inhibition, there is no report to explore the systematic mechanism, but it is suggested that by cytotoxic effects, the active compounds tend to hinder a specific kinase by creating pressure on the cell to realize resistance through mutations in the kinase gene that abolish drug [54]. The protein kinase inhibition study of the organotin(IV) complexes is shown in Fig 10, reflecting the degree of inhibition and the formation of inhibition zones in the range of 8.0-10.0 mm. The kinase study suggested that the complex (5) is more operative and produces the largest inhibition zones on the culture plates, and might be used as an active drug to prevent the growth of tumours [15].

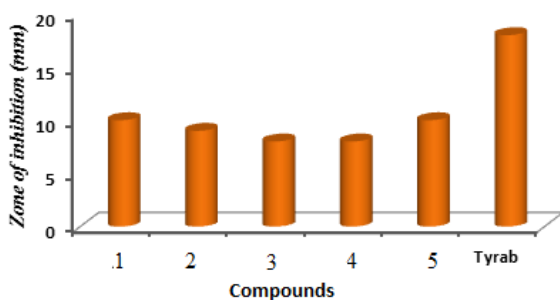


Fig. 10: Protein kinase inhibition assay of organotin(IV) complexes.

Structure-activity relationship

Organotin complexes with significant bactericidal activity were examined in comparison to free ligand, which are related to increased lipid solubility and penetration through the cell membrane. To correlate the biological studies in terms of structure-activity relationships, the results established that the bioactivity of organotin(IV) derivatives strongly be influenced by the accessibility of coordination sites at tin [55]. Further, the bactericidal activity is dependent on ligand-to-metal coordination. As a result of interaction, the polarizability of tin reduces due to the delocalization of π -electrons and the sharing of positive charges to the donor species [53]. Also, due to strong coordination, the lipophilicity of tin increased, which supported a linear increase in the permeability through the plasma membrane. When compared to other alkyl groups, tributyltin had the strongest inhibitory effect on fungus. The enhancement in antifungal activity was ascribed to the tributyl groups linked to the Sn atom. The excellent activities of the complexes depend upon the degree of coordination between tin and sulfur. Triorganotin was found to be more effective than diorganotin against fungi due to the presence of four coordinated

geometry, which increases the antifungal activity of triorganotin complexes. To reduce the fungicidal activity of organotin complexes, several parameters, like steric hindrance and electronic constraints enforced by organometallic species, were addressed [52,56, 60].

Conclusion

The effective organotin(IV) based *oxo*-ethyl carbonodithioate derivatives were synthesized and confirmed by applying several techniques, including FT-IR, NMR (^1H , ^{13}C), AFM, DFT studies, and UV-visible spectrophotometry. To assess the role of alkyl/phenyl groups on the activity of organotin derivatives in terms of the structure-activity relationship, the complexes were evaluated *in vitro* against typical microbial strains. The AFM results suggested highly rough surfaces with significant RMS values, available for a variety of interactions at the cellular and molecular level as a chemotherapeutic drug. The DFT analysis revealed the internal parameters in terms of HOMO-LUMO energy gaps, electrophilicity, and bond energies are attractive parameters for further consideration as pre-determined parameters for hi-tech targeted interactions. The biocidal performance of organotin(IV) *oxo*-ethyl carbonodithioate derivatives was confirmed by testing against various microbial strains. The *in vitro* ligand-DNA binding capabilities and thermodynamic stability address the success of such complexes for targeted application at molecular and cellular levels in the pharmaceutical, cosmetic, and biocatalytic industries.

Acknowledgement

Fatima Javed (PIN # 117-7469-PS7-018), is highly grateful to the Higher Education Commission Pakistan, for sponsoring this research.

References

1. S. Singh, S. Bhattacharya, H. Nöth, Synthesis and Structural Studies of Organotin (IV) and Organolead (IV) Thiophene-2-thiocarboxylate, *Eur. J. Inorg. Chem.*, **36**, 5691 (2010).
2. S. Hussain, S. Ali, S. Shahzadi, M. N. Tahir, M. Shahid, K. S. Munawar, S. M. Abbas, Synthesis, spectroscopy, single crystal XRD and biological studies of multinuclear organotin dicarboxylates, *Polyhedron*, **117**, 64 (2016).
3. F. Javed, M. Sirajuddin, S. Ali, N. Khalid, M.N. Tahir, N.A. Shah, Z. Rasheed, M.R. Khan, Organotin (IV) derivatives of *o*-isobutyl carbonodithioate: Synthesis, spectroscopic characterization, X-ray structure, HOMO/LUMO

- and in vitro biological activities, *Polyhedron*, **104**, 80 (2016).
- S. Hussain, I. H. Bukhari, S. Ali, S. Shahzadi, M. Shahid, K. S. Munawar, Synthesis and spectroscopic and thermogravimetric characterization of heterobimetallic complexes with Sn (IV) and Pd (II); DNA binding, alkaline phosphatase inhibition and biological activity studies, *J. Coord. Chem.*, **68**, 662 (2015).
 - F. Javed, S. Ali, S. Shahzadi, S.K. Sharma, K. Qanungo, M.N. Tahir, N.A. Shah, M.R. Khan, N. Khalid, Synthesis, structural characterization, theoretical calculations and in vitro biological activities of organotin (IV) complexes with [O, O] donor ligand, *J. Inorg. Organomet. Polym. Mater.*, **26**, 48 (2016).
 - F. Javed, S. Ali, S. Shahzadi, M. Tahir, S. Tabassum, N. Khalid, Organotin(IV) *O*-butyl carbonodithioates: Synthesis, characterization, *in vitro* bioactivities, and interaction with SS-DNA, *Russ. J. Gen. Chem.*, **86** 2768 (2016).
 - B. Hanifa, M. Sirajuddin, E.R. Tiekink, I. Khan, M. Kubicki, A. Bari, Journal of Molecular Structure, 1260 (2022) 132814.
 - M. Sirajuddin, S. Ali, M.N. Tahir, Journal of Molecular Structure, 1229 (2021) 129600.
 - N. Muhammad, M. Ahmad, M. Sirajuddin, Z. Ali, N. Tumanov, J. Wouters, A. Chafik, K. Solak, A. Mavi, S. Muhammad, *Frontiers in Pharmacology*, **13** (2022) 864336.
 - J.B. Graceli, G.C. Sena, P.F.I. Lopes, G.C. Zamprogno, M.B. da Costa, A.F.L. Godoi, D.M. dos Santos, M.R.R. de Marchi, M.A. dos Santos Fernandez, Organotins: a review of their reproductive toxicity, biochemistry, and environmental fate, *Reprod. Toxicol.*, **36**, 40 (2013).
 - F. Maqbool, S. Mostafalou, H. Bahadar, M. Abdollahi, Review of endocrine disorders associated with environmental toxicants and possible involved mechanisms, *Life Sci.*, **145**, 265 (2016).
 - F. Javed, S. Ali, S. Shahzadi, S. K. Sharma, K. Qanungo, K. S. Munawar, I. Khan, Synthesis, characterization, and biological activity of organotin(IV) complexes with 4-oxo-4-[3-(trifluoromethyl)phenylamino]butanoic acid, *Russ. J. Gen. Chem.*, **87**, 2409 (2017).
 - Y. Yan, J. Zhang, L. Ren, C. Tang, Metal-containing and related polymers for biomedical applications, *Chem. Soc. Rev.*, **45**, 5232 (2016).
 - S.K. Hadjikakou, N. Hadjiliadis, Antiproliferative and anti-tumor activity of organotin compounds, *Coord. Chem. Rev.*, **253**, 235 (2009).
 - S. Tabassum, C. Pettinari, Chemical and biotechnological developments in organotin cancer chemotherapy, *J. organomet. Chem.*, **691**, 1761 (2006).
 - F. Javed, S. Ali, S. Shahzadi, S. Sharma, K. Qanungo, K. Munawar, I. Khan, *Russian Journal of General Chemistry*, **87** (2017) 2409-2420.
 - F. Javed, S. Ali, M.W. Shah, K.S. Munawar, S. Shahzadi, Hameedullah, H. Fatima, M. Ahmed, S.K. Sharma, K. Qanungo, Synthesis, characterization, semi-empirical study, and biological activities of organotin (IV) and transition metal complexes with *o*-methyl carbonodithioate, *J. Coord. Chem.*, **67**, 2795 (2014).
 - W.L. F. Armarego, C.L.L. Chai, *Purification of Laboratory Chemicals*, London: Butterworth Heinemann, 5th ed., Oxford, UK, (2003).
 - F. Ullah, F. Javed, M.B.H. Othman, Z. Ahmad, H.M. Akil, Synthesis and physicochemical investigation of chitosan-built hydrogel with induced glucose sensitivity, *Int. J. Polym. Mater. Polym. Biomater.*, **66**, 824 (2017).
 - A.T. Paulino, M.R. Guilherme, E.A. de Almeida, A.G. Pereira, E.C. Muniz, E.B. Tambourgi, One-pot synthesis of a chitosan-based hydrogel as a potential device for magnetic biomaterial, *J. Magn. Magn. Mater.*, **321**, 2636 (2009).
 - K. Ramasamy, V.L. Kuznetsov, K. Gopal, M.A. Malik, J. Raftery, P.P. Edwards, P. O'Brien, Organotin dithiocarbamates: single-source precursors for tin sulfide thin films by aerosol-assisted chemical vapor deposition (AACVD), *Chem. Mater.*, **25**, 266 (2013).
 - A. Kana, T. Hibbert, M. Mahon, K. Molloy, I. Parkin, L. Price, Organotin unsymmetric dithiocarbamates: synthesis, formation and characterisation of tin (II) sulfide films by atmospheric pressure chemical vapour deposition, *Polyhedron*, **20**, 2989 (2001).
 - S. Cheng, Y. Chen, Y. He, G. Chen, The structure and properties of SnS thin films prepared by pulse electro-deposition, *Mater. Lett.*, **61**, 1408 (2007).
 - M. Frisch, G. Trucks, H. Schlegel, G. Scuseria, M. Robb, J. Cheeseman, J. Montgomery Jr, T. Vreven, K. Kudin, J. Burant, Millam JM. Gaussian 03, Revision C. 02. Wallingford, CT: Gaussian. Inc. (2004).
 - K. S. Munawar, S. Ali, M. N. Tahir, N. Khalid, Q. Abbas, I. Z. Qureshi, S. Shahzadi, Investigation of derivatized Schiff base ligands of 1, 2, 4-triazole amine and their oxovanadium (IV) complexes: synthesis, structure, DNA binding, alkaline phosphatase inhibition, biological screening, and insulin mimetic properties, *Russ. J. Gen. Chem.*, **85**, 2183 (2015).
 - N. Singh, S. Bhattacharya, Synthesis and characterization of some triorgano, diorgano,

- monoorganotin and a triorganolead heteroaromatic dithiocarbamate complexes, *J. Organomet. Chem.*, **700**, 69 (2012).
27. S. Hussain, S. Ali, S. Shahzadi, M.N. Tahir, M. Shahid, Synthesis, characterization, single crystal XRD and biological screenings of organotin (IV) derivatives with 4-(2-hydroxyethyl) piperazine-1-carbodithioic acid, *J. Coord. Chem.*, **69**, 687 (2016).
 28. G. Domazetis, R. Magee, B. James, Synthesis and structure of some triphenyltin (IV) dithiocarbamate compounds, *J. Organomet. Chem.*, **141**, 57 (1977).
 29. S. Shahzadi, S. Ali, K. Wurst, M. Najam-ul-Haq, Synthesis of stannic (IV) complexes: Their structural elucidation in solid and solution state and antimicrobial activity, *Heteroat. Chem.*, **18**, 664 (2007).
 30. R. Willem, I. Verbruggen, M. Gielen, M. Biesemans, B. Mahieu, T.S. Basu Baul, E.R. Tiekink, Correlating Mössbauer and solution-and solid-state ^{117}Sn NMR data with X-ray diffraction structural data of triorganotin 2-[(E)-2-(2-hydroxy-5-methylphenyl)-1-diazenyl] benzoates, *Organometallics*, **17**, 5758 (1998).
 31. L.A. Gómez-Ortiz, R. Cea-Olivares, V. García-Montalvo, S. Hernández-Ortega, Dimeric dithiocarbamates of stannolane. An example of the presence of secondary bonds in the formation of an inorganic ring. Molecular and crystal structure of 2-nbutyl-2-(dimethyldithiocarbamate)-1, 3, 2-oxathiaannolane and 2-nbutyl-2-(piperidyldithiocarbamate)-1, 3, 2-oxathiaannolane, *J. Organomet. Chem.*, **654**, 51 (2002).
 32. A. Tarassoli, T. Sedaghat, B. Neumüller, M. Ghassemzadeh, Synthesis, spectroscopic investigations and crystal structures of organotin (IV) derivatives of 2-amino-1-cyclopentene-1-carbodithioic acid, *Inorganica Chim. Acta*, **318**, 15 (2001).
 33. N. Muhammad, S. Shuja, S. Ali, I.S. Butler, A. Meetsma, M. Khan, New dimeric, trimeric and supramolecular organotin (IV) dithiocarboxylates: synthesis, structural characterization and biocidal activities, *Polyhedron*, **28**, 3439 (2009).
 34. T.P. Lockhart, W.F. Manders, E.M. Holt, Solution and solid-state molecular structures of $\text{Me}_2\text{Sn}(\text{OAc})_2$ and its hydrolyzate, $([\text{Me}_2\text{Sn}(\text{OAc})]_2\text{O})_2$, by solution and solid-state carbon-13 NMR. X-ray diffraction study of the hydrolyzate. *J. Am. Chem. Soc.*, **108**, 6611 (1986).
 35. G. Barone, T.G. Hibbert, M.F. Mahon, K.C. Molloy, L.S. Price, I.P. Parkin, A.M. Hardy, M.N. Field, Deposition of tin sulfide thin films from tin (IV) thiolate precursors, *J. Mater. Chem.*, **11**, 464, (2001).
 36. M.M. Ali, G.A. El-Hiti, E. Yousif, Photostabilizing efficiency of poly (vinyl chloride) in the presence of organotin (IV) complexes as photostabilizers, *Molecules*, **21**, 1151 (2016).
 37. C. An, K. Tang, G. Shen, C. Wang, Q. Yang, B. Hai, Y. Qian, Growth of belt-like SnS crystals from ethylenediamine solution, *J. Cryst. Growth*, **244**, 333 (2002).
 38. S. Basu, G. Gupta, B. Das, K.M. Rao, Neutral penta-coordinated diorganotin (IV) complexes derived from ortho-aminophenol Schiff bases: Synthesis, characterization and molecular structures, *J. Organomet. Chem.*, **695**, 2098 (2010).
 39. S. Pokharia, Theoretical insights on organotin (IV)-protein interaction: density functional theory (DFT) studies on di-n-butyltin (IV) derivative of glycylvaline, *Asian J. Res. Chem.*, **8**, 7 (2015).
 40. Y.-Z. Xie, G.-G. Shan, P. Li, Z.-Y. Zhou, Z.-M. Su, A novel class of Zn (II) Schiff base complexes with aggregation-induced emission enhancement (AIEE) properties: Synthesis, characterization and photophysical/electrochemical properties, *Dyes and Pigm.*, **96**, 467 (2013).
 41. H. Kargar, M. N. Jahromi, M. F. Mehrjardi, R. B. Ardakani, K. S. Munawar, S. Ali, M. Ashfaq, M. N. Tahir, Synthesis, spectral characterization, crystal structure and catalytic activity of a novel dioxomolybdenum Schiff base complex containing 4-aminobenzhydrazone ligand: A combined experimental and theoretical study, *J. Mol. Struct.*, **1249**, 131645 (2022).
 42. H. Kargar, M. F. Mehrjardi, R. B. Ardakani, K. S. Munawar, M. Ashfaq, M. N. Tahir, Diverse coordination of isoniazid hydrazone Schiff base ligand towards iron (III): Synthesis, characterization, SC-XRD, HSA, QTAIM, MEP, NCI, NBO and DFT study, *J. Mol. Struct.*, **1250**, 131691, (2022).
 43. R.G. Pearson, Chemical hardness and density functional theory, *J. Chem. Sci.*, **117**, 369 (2005).
 44. M. F. Mehrjardi, H. Kargar, R. B. Ardakani, M. Ashfaq, K. S. Munawar, M. N. Tahir, Symmetrical Pd (II) and Ni (II) Schiff base complexes: Synthesis, crystal structure determination, spectral characterization, and theoretical studies, *J. Mol. Struct.*, **1251**, 132037 (2021).
 45. M. Ashfaq, M. N. Tahir, S. Muhammad, K. S. Munawar, A. Ali, G. Bogdanov, S. S. Alarfaji,

- Single-crystal investigation, Hirshfeld surface analysis, and DFT study of third-order NLO properties of unsymmetrical acyl thiourea derivatives, *ACS Omega* **6**, 31211 (2021).
46. K. S. Munawar, S. Ali, M. N. Tahir, N. Khalid, Q. Abbas, I. Z. Qureshi, S. Hussain, M. Ashfaq, Synthesis, spectroscopic characterization, X-ray crystal structure, antimicrobial, DNA-binding, alkaline phosphatase and insulin-mimetic studies of oxidovanadium (IV) complexes of azomethine precursors, *J. Coord. Chem.*, **73**, 2275 (2020).
 47. F. Javed, S. Ali, S. Shahzadi, S.K. Sharma, K. Qanungo, M.N. Tahir, N.A. Shah, M.R. Khan, N. Khalid, *Journal of Inorganic and Organometallic Polymers and Materials*, **26** (2016) 48-61.
 48. M. Zaheer, A. Shah, Z. Akhter, R. Qureshi, B. Mirza, M. Tauseef, M. Bolte, Synthesis, characterization, electrochemistry and evaluation of biological activities of some ferrocenyl Schiff bases, *Appl. Organomet. Chem.*, **25**, 61 (2011).
 49. S. T. Hafeez, M. N. Tahir, S. Ali, M. Iqbal, H. Gulab, K. S. Munawar, One-pot synthesis, characterization, DNA binding and enzymatic studies of 4-methyl trans-cinnamate zinc (II)-mixed ligand complexes, *J. Coord. Chem.*, **68**, 3636 (2015).
 50. X.-Y. Zhang, H.-B. Song, Q.-S. Li, X.-F. Liu, L.-F. Tang, Synthesis, structure and biological activity of organotin derivatives with pyridylmethylthiobenzoic acid, *Polyhedron*, **26**, 3743 (2007).
 51. Y. Shi, B.-Y. Zhang, R.-F. Zhang, S.-L. Zhang, C.-L. Ma, Syntheses, characterizations, crystal structures, and in vitro antitumor activities of chiral triorganotin (IV) complexes containing (S)-(+)-2-(4-isobutyl-phenyl) propionic and (R)-(+)-2-(4-hydroxyphenoxy) propionic acid ligands, *J. Coord. Chem.*, **65**, 4125 (2012).
 52. M. Tariq, N. Muhammad, M. Sirajuddin, S. Ali, N.A. Shah, N. Khalid, M.N. Tahir, M.R. Khan, Synthesis, spectroscopic characterization, X-ray structures, biological screenings, DNA interaction study and catalytic activity of organotin (IV) 3-(4-fluorophenyl)-2-methylacrylic acid derivatives, *J. organomet. Chem.*, **723**, 79 (2013).
 53. R. Jahan, M. Yousaf, H. Khan, S.A. Shah, A.A. Khan, N. Bibi, F. Javed, M. Ijaz, A. Ali, D.-Q. Wei, *Journal of Neuroimmune Pharmacology*, (2023) 1-12.
 54. N. Muhammad, S. Ali, I.S. Butler, A. Meetsma, New mononuclear organotin (IV) 4-benzhydrylpiperazine-1-carbodithioates: synthesis, spectroscopic characterization, X-ray structures and in vitro antimicrobial activities, *Inorganica Chim. Acta*, **373**, 187 (2011).
 55. D.N. Nicolaides, D.R. Gautam, K.E. Litinas, D.J. Hadjipavlou-Litina, K.C. Fylaktakidou, Synthesis and evaluation of the antioxidant and antiinflammatory activities of some benzo [1] khellactone derivatives and analogues, *Eur. J. Med. Chem.*, **39**, 323 (2004).
 56. J. Zhang, P.L. Yang, N.S. Gray, Targeting cancer with small molecule kinase inhibitors, *Nat. Rev. Cancer*, **9**, 28 (2009).
 57. S. Shoaib Ahmad Shah, M. Ashfaq, A. Waseem, M. Mehboob Ahmed, T. Najam, S. Shaheen, G. Rivera, Synthesis and Biological Activities of Organotin (IV) Complexes as Antitumoral and Antimicrobial Agents. A Review, *Mini Rev. Med. Chem.*, **15**, 406 (2015).
 58. W. Rehman, M. Baloch, A. Badshah, S. Ali, Synthesis and in vitro fungicidal study of organotin (IV) complexes of monomethyl glutarate, *Russ. J. Coord. Chem.*, **31**, 856 (2005).
 59. H. Ullah, V. Previtali, H.B. Mihigo, B. Twamley, M.K. Rauf, F. Javed, A. Waseem, R.J. Baker, I. Rozas, *European Journal of Medicinal Chemistry*, **181** (2019) 111544.